DESIGN AND OPTIMIZATION OF A FUZZY-PID CONTROLLER USING A GENETIC ALGORITHM FOR OVERHEAD CRANE CONTROL

Nguyễn Văn Trung[1,*], Nguyễn Thị Phúc[1], Phí Thị Thanh Huyền[1], Trần Thị Duyên[1], Đỗ Minh Hiếu[2]

[1]*Trường Đại học Công nghiệp Quảng Ninh*

[2]*Công Ty TNHH điện lực AES Mông Dương*

[*]Email: ngvtrung1982@gmail.com

ABSTRACT:

An overhead crane (OC) is an electromechanical system with nonlinear dynamics and is significantly affected by load oscillations (LO), which are commonly modeled as a double-pendulum (D-P) system. Oscillations (O) of the hook and payload (H&P) degrade trolley (T) positioning (P) accuracy and may lead to mechanical damage and safety hazards. To mitigate these limitations, a combined FLC–PID control scheme is introduced with the aim of improving the operational performance of an OC. In the proposed scheme, the fuzzy controller enhances the system's dynamic response under large tracking errors, thereby ensuring fast positioning of the T at the desired location. The PID controller ensures system stability as the T approaches the setpoint, employing a genetic algorithm (GA) to optimize parameters for oscillation suppression and P accuracy enhancement. The effectiveness of the proposed approach is validated through MATLAB/Simulink simulations. Simulation results demonstrate improved P accuracy, significant reduction of H&P O, and fast, stable system responses.

Keywords: *Overhead crane; Fuzzy and PID control; Genetic algorithm; Oscillation control; Positioning.*

1. INTRODUCTION

Double-pendulum OC systems are indispensable lifting devices in modern logistics and industrial applications, including container terminals, construction sites, metallurgical plants, and heavy manufacturing lines. Owing to their ability to transport and position heavy payloads within constrained workspaces, overhead cranes play a critical role in improving productivity and reducing operational costs. However, the increasing demand for higher operating speed, positioning accuracy, and safety has significantly complicated the control problem. An effective control system must not only ensure fast and accurate trolley positioning but also simultaneously suppress the swing motions of the hook and the payload, which are major sources of positioning errors, mechanical wear, and safety risks in practical operations.

An OC system, from a structural and dynamic standpoint, consists of a T that moves horizontally, a hook (H) suspended from the T through a cable, and a payload (P) connected to the H [1–6], as illustrated in Figure 1. During trolley motion, the inertia of the H&P induces oscillatory behavior, resulting in a strongly nonlinear system with tight coupling between translational and rotational motions. In many practical scenarios, especially when the cable length varies or the payload mass is non-negligible, the crane's dynamic behavior is more accurately represented by a D–P model [7]. These O not only degrade lifting and transportation efficiency but also adversely affect positioning accuracy and the service life of mechanical components. Moreover, in real industrial environments, OC operate under uncertain conditions arising from P variations, friction, wind disturbances, and external excitations, and parameter mismatches, which further increase the complexity of the control problem.

In recent years, several advanced control methods have been proposed to enhance the operational performance of OC systems, including adaptive control [8], input shaping [9], sliding mode control (SMC) [10], and fuzzy sliding mode control (FSMC) [11–12]. These approaches have demonstrated improved stability and robustness under disturbances and uncertainties. Meanwhile, the effectiveness of FLC in handling nonlinearities and uncertainties in OC systems has been widely reported [13]. Dual fuzzy PD control structures, in which one controller focuses on trolley positioning while the other suppresses payload oscillations, have achieved promising results [14]. However, many dual fuzzy control approaches [15] involve a trade-off between swing reduction and large overshoot, leading to prolonged settling times and limiting their applicability in fast industrial operations.

Alongside intelligent control methods, PID controllers remain dominant in industrial applications due to their simple structure, ease of implementation, and high reliability. To enhance PID performance, various optimization algorithms have been employed for parameter tuning, such as PSO [16], DE [17], and GA [18]. More recently, the Fuzzy-PID control structure has emerged as a hybrid approach that combines the advantages of classical and intelligent control techniques. In such schemes, the fuzzy controller provides fast responses under large tracking errors, while the PID controller ensures stability and high precision near the desired operating point [19–20]. Nevertheless, most existing studies focus primarily on overhead crane systems modeled as single-pendulum systems, which do not fully capture the dynamics encountered in real industrial applications.

Motivated by these practical considerations and the aforementioned limitations, this paper proposes a novel control structure that integrates a fuzzy logic controller with two PID controllers for a D-P OC system, where a GA is used to optimally tune the PID controller parameters. The proposed approach aims to shorten the system response time, significantly reduce the swing angles (SA) of both the H&P, and enhance trolley positioning accuracy under realistic operating conditions. Simulation results obtained in the MATLAB/Simulink (M/S) environment confirm the effectiveness and robustness of the proposed controller.

The organization of this paper is outlined as follows. In Section 2, the dynamic modeling of the OC system is presented. Section 3 focuses on the design of the FLC–PID controller optimized using a GA. Section 4 provides a discussion and analysis of the simulation results, while Section 5 concludes the paper.

Figure 1. Schematic of the D-P OC system

2. DYNAMIC MODELING OF THE OC SYSTEM

The D-P OC system is illustrated in Figure 2, where the technical parameters and their corresponding values are selected based on practical operating conditions, as shown in Table 1. The OC system is modeled as a T with mass M, a H with mass m_1, and a P with mass m_2. The lengths of the H cable and the P cable are denoted by l_1 and l_2, respectively. The SA of the H&P are represented by $y_1$and y_2, while their corresponding angular velocities are $\dot{y}_1$and $\dot{y}_2$.

During operation, the overhead crane moves horizontally under the action of a control force F (N) and is subjected to external disturbances denoted by $d(t)$. In the modeling process, the cables are assumed to be rigid, massless, and inextensible.

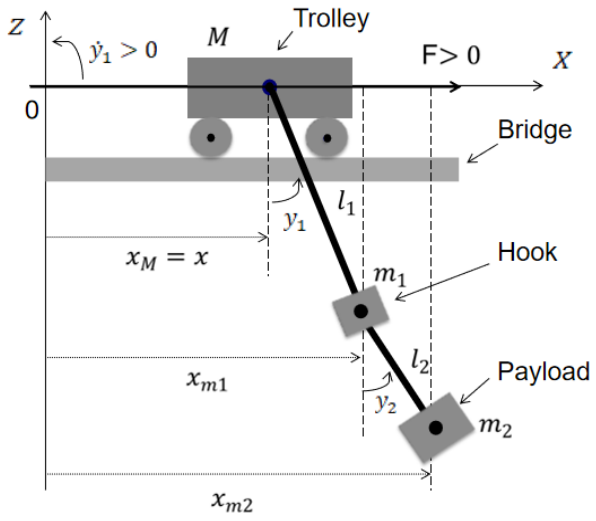

Figure 2. Configuration of the OC system

Table 1. OC system symbols and parameter values

Symbol	Describe	Value
M (Kg)	Weight of T	24
m_1 (Kg)	Weight of H	7
m_2 (Kg)	Weight of P	12
l_1 (m)	Length of cable H	2
l_2(m)	Length of cable P	0.6
g (m/s2)	Gravity acceleration	9.81
μ	Coefficient of friction	0.2

Using Lagrange's method [11], the dynamic behavior of the system is described by the following equations:

$$\frac{d}{dt}\left(\nabla_{\dot{q}_j} L\right) = \nabla_{q_j} L + Q_j \quad (1)$$

where Q_j accounts for the effect of external generalized forces, q_j denotes the generalized coordinate, j is the number of degrees of freedom of the crane system, $L = G_d - G_t$ is the Lagrangian, G_t is the potential energy, G_d is the crane's kinetic energy (KE).

$$G_{\mathrm{d}} = \sum_{i=1}^{n} \frac{1}{2} m_i \dot{x}_i^2 \quad (2)$$

The position coordinates of the T, H&P, as depicted in Fig. 2, are given by:

$$x_{m_{i'}} = x + \sum_{j=1}^{i'} l_j\, Y_j, i' = 0,1,2, \quad (3)$$

with $x_{m_0} \equiv x_M = x,\ Y_1 = siny_1; Y_2 = siny_2$

The motion of the T, H&P yields the following velocity components:

$$\dot{x}_{m_{i'}} = \dot{x} + \sum_{j=1}^{i'} l_j\, \dot{y}_j Y_{j+2}, i' = 0,1,2, \quad (4)$$

with $\dot{x}_{m_0} \equiv \dot{x}_M = \dot{x},\ Y_3 = cosy_1; Y_4 = cosy_2$

The OC system's KE is given by:

$$\begin{aligned} G_{\mathrm{d}} &= G_{\mathrm{d}_M} + G_{\mathrm{d}_{m1}} + G_{\mathrm{d}_{m2}} = \tfrac{1}{2} M \dot{x}^2 \\ &+ \tfrac{1}{2} m_i \left(\dot{x}^2 + l_i^2 \dot{y}_i^2 + 2\dot{x} l_i \dot{y}_i Y_{2i+1}\right) \\ &+ \tfrac{1}{2} m_j (\dot{x}^2 + l_i^2 \dot{y}_i^2 + l_j^2 \dot{y}_j^2 + 2\dot{x} l_i \dot{y}_i Y_{2i+1} \\ &+ 2\dot{x} l_j \dot{y}_j Y_{j+2} + 2 l_i l_j \dot{y}_i \dot{y}_j Y_{j+4}) \end{aligned} \quad (5)$$

Where: $i = 1, j = 2, Y_{j+4} = cos(y_1 - y_2)$

The potential energy of the overhead crane system is given by:

$$G_{\mathrm{t}} = \tilde{\mathrm{m}} g l_i (1 - Y_{2i+1}) + m_j g l_j \left(1 - Y_{2j+2}\right) \quad (6)$$

Where: $i = 1, j = 2, \tilde{\mathrm{m}} = m_1 + m_2$

The nonlinear dynamics of the OC system can be derived by substituting (5) and (6) into (1) [11]:

$$\begin{aligned} &M_i \ddot{x} + M_j (\ddot{y}_i Y_{2i+1} - \dot{y}_i^2 Y_i) \\ &+ M_{2i+1} \left(\ddot{y}_j Y_{j+2}) - \dot{y}_j^2 Y_j\right) = F + F_d - F_{rx} \end{aligned} \quad (7)$$

$$\begin{aligned} &M_j Y_{2i+1} \ddot{x} + M_{j+2} \ddot{y}_i + M_{j+3} \ddot{y}_j Y_{j+4} \\ &+ M_{j+3} \dot{y}_j^2 Y_{j+3} + M_j g Y_i = F_{yi} \end{aligned} \quad (8)$$

$$\begin{aligned} &M_{2i+1} Y_{j+2} \ddot{x} + M_{j+3} \ddot{y}_i Y_{j+4} + M_{j+4} \ddot{y}_j \\ &- M_{j+3} \dot{y}_i^2 Y_{j+3} + M_{2i+1} g Y_j = F_{yj} \end{aligned} \quad (9)$$

The system parameters are defined as follows: $i = 1, j = 2,\ M_1 = M + \tilde{\mathrm{m}}, \check{\mathrm{I}} = l_1 l_2,\ M_2 = \tilde{\mathrm{m}} l_1, M_3 = m_2 l_2, M_4 = \tilde{\mathrm{m}} l_1^2, M_5 = m_2 \check{\mathrm{I}}, M_6 = m_2 l_2^2, Y_5 = \sin(y_1 - y_2)$.

The force F is used as the system input driving the trolley motion. The friction force between the trolley and the bridge is denoted by F_{rx}. In addition, aerodynamic drag forces acting on the trolley and the payload are represented by F_d, F_{y_1}, and F_{y_2}, respectively.

The state vector is defined as a mapping $X: \mathbb{R}_{\geq 0} \to \mathbb{R}^6$, such that:

$$X(t) = (x(t), y_1(t), y_2(t), \dot{x}(t), \dot{y}_1(t), \dot{y}_2(t)),$$

The system is driven by the control force $u(t) = F$, whereas the effects of friction and aerodynamic drag are represented through the disturbance vector $d(t) = \left(di(t)\right)_{i=1}^{4}$, $d_1 = F_{rx}$, $d_2 = F_d$, $d_3 = F_{y_1}$, $d_4 = F_{y_2}$.

From the above:

$$\dot{X}(t) = \tau(X) + ב(X)u(t) + \breve{\aleph}(X)d(t) \quad (10)$$

Where: Let $\tau(X) = (\tau_i(X))_{i=1}^{6}$ and

$$ב(X) = (ב_i(X))_{i=1}^{6} \quad (11)$$

are non-linear functions,

$\breve{\aleph}(X) = \begin{bmatrix} 0 \\ \breve{\aleph}_{\varphi j} \end{bmatrix}$, $\breve{\aleph}_{\varphi j} = \begin{bmatrix} \breve{\aleph}_{\varphi\gamma} & \breve{\aleph}_{\varphi\delta} \end{bmatrix}, \varphi = 4,5,6, \gamma = 1,2, \delta = 3,4$ are the outer bound disturbances of wind and collision.

Where:

$$\breve{\aleph}_{41} = M_4M_6 - M_5^2Y_6^2/w(X), \quad (12)$$

$$\breve{\aleph}_{42} = -M_4M_6 + M_5^2Y_6^2/w(X), \quad (13)$$

$$\breve{\aleph}_{43} = M_2M_6Y_3 - M_3M_5Y_4Y_6/w(X), \quad (14)$$

$$\breve{\aleph}_{44} = M_3M_4Y_4 - M_2M_5Y_3Y_6/w(X), \quad (15)$$

$$\breve{\aleph}_{51} = -M_2M_6Y_3 + M_3M_5Y_4Y_6/w(X), \quad (16)$$

$$\breve{\aleph}_{52} = M_2M_6Y_3 - M_3M_5Y_4Y_6/w(X), \quad (17)$$

$$\breve{\aleph}_{53} = -M_1M_6 + M_3^2Y_6^2/w(X), \quad (18)$$

$$\breve{\aleph}_{54} = M_1M_5Y_6 - M_2M_3Y_3Y_4/w(X), \quad (19)$$

$$\breve{\aleph}_{61} = -M_3M_4Y_4 + M_2M_5Y_3Y_6/w(X), \quad (20)$$

$$\breve{\aleph}_{62} = M_3M_4Y_4 - M_2M_5Y_3Y_6/w(X), \quad (21)$$

$$\breve{\aleph}_{63} = M_1M_5Y_6 - M_2M_3Y_3Y_4/w(X), \quad (22)$$

$$\breve{\aleph}_{64} = -M_1M_4 + M_2^2Y_3^2/w(X), \quad (23)$$

$$w(X) = M_2^2M_6Y_4^2 - M_1M_4M_6 + M_3^2M_4Y_4^2 + M_1M_5^2Y_6^2 - 2M_2M_3M_5Y_3Y_4bY_6. \quad (24)$$

The OC system dynamic model considered here differs from that in [11]. Specifically, the model in [11] represents the crane system as a single-pendulum configuration and does not account for external disturbances such as wind or collision effects. Moreover, in that model, the disturbance term $א(X)$ and the functions $\tau(X)$and $ב(X)$are assumed to be linear.

3. DESIGN OF THE FLC-PID CONTROLLER

Considering the nonlinear and under-actuated characteristics of the OC system, a GA is utilized to optimally tune the PID controller parameters, thereby improving control performance. The GA-optimized PID controller is integrated with a fuzzy logic controller (FLC) to form a hybrid FLC–PID control structure, which combines the flexibility and strong nonlinear handling capability of FLC with high level of precision and stability of PID in the vicinity of the setpoint.

The design of the hybrid controller relies on the tracking error ε(t) and its derivative ε̇(t). The FLC exhibits superior performance in regions with large tracking errors, where its nonlinear characteristics enable rapid dynamic responses. As the system state approaches the desired setpoint, i.e., when both $\varepsilon(t)$ and $\dot{\varepsilon}(t)$approach zero, the influence of the fuzzy controller is gradually reduced, and the PID controller becomes dominant to ensure accurate steady-state performance.

The optimal FLC–PID controller produces a time-domain composite control signal, which is given by:

$$u(t) = \tilde{\emptyset}u_{FLC}(t) + \left(1 - \tilde{\emptyset}\right)u_{PID}(t) \quad (25)$$

Where: $u_{PID}(t)$ corresponds to the control signal generated by the GA-optimized PID, $u_{FLC}(t)$ represents the FLC signal, and $\tilde{\emptyset} \in [0,1]$ is the switching weight function determined by the FLC ($\tilde{\emptyset} = 1$ favors FLC; $\tilde{\emptyset} = 0$ favors PID).

The transition between the FLC and PID control regions can be achieved using either a fuzzy switch or the FLC itself. When the FLC is employed for switching, it additionally monitors the system behavior to determine the appropriate transition. The switching between FLC and PID can be governed by the following rules:

If $|\varepsilon_i(t)|$is large and $|\dot{\varepsilon}_i(t)|$is large, then the FLC is given priority.

$$u(t) = u_{FLC}(t) \quad (26)$$

If $|\varepsilon_i(t)|$is small and $|\dot{\varepsilon}_i(t)|$is small, then priority is assigned to the PID.

$$u(t) = u_{PID}(t) \quad (27)$$

If the system exhibits potential oscillatory behavior, the PID control action is attenuated.

The overhead crane system involves three

critical control variables: x_1(TP), x_3 (HS), and x_5 (PS). These variables are regulated with respect to their reference setpoints. Let x_r1 and x_r3 denote the target TP and HSA, while x_1 and x_3 denote the actual system responses. The resulting control errors are defined as follows:

$$\varepsilon_i = x\_ri - x_i \quad (28)$$

$$\varepsilon_j = x_{j+1} - x\_r(j+1) \quad (29)$$

Where: $i = 1, j = 2$

The control objective of the FLC-PID controller is to ensure that, under the action of $u(t)$, the errors between x_1, x_3 and their reference values x_r1, x_r3 converge to zero as $t \to \infty$, while minimizing payload swing.

$$\lim_{t\to\infty} \varepsilon_1(t) = 0 \quad (30)$$

$$\lim_{t\to\infty} \varepsilon_2(t) = 0 \quad (31)$$

The time-domain overall control signal of the FLC–PID controller is given by:

$$u(t) = \tilde{\emptyset} u_{FLC}(t) + \left(1 - \tilde{\emptyset}\right)\left(u_{PID1}(t) + u_{PID2}(t)\right) \quad (32)$$

According to Eq. (18), Figure 3 depicts the schematic of the FLC–PID controller applied to the D-P OC system.

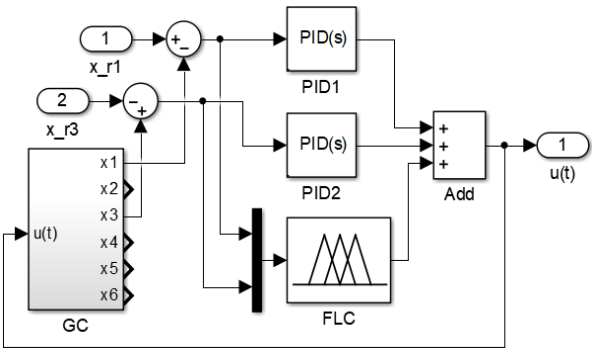

Figure 3. M/S-based block diagram of the FLC–PID controller applied to the D-P OC system.

3.1. Design of the FLC Controller

To control the D-P OC system, a FLC based on experience-driven IF–THEN (I-T) rules is employed. The FLC designed for this system utilizes two input linguistic variables and one output linguistic variable, with each variable's universe of discourse evenly partitioned into the following ranges:

Input 1: Trolley position error:

$$\rho_1(t) \in [-4, 4] \text{ (m)}$$

Input 2: Hook swing angle error:

$$\rho_2(t) \in [-0.1, 0.1] \ (rad)$$

Output: his constitutes the FLC output signal, defined over the following range of values:

$$u_{FLC}(t) \in [-18, 18] \ (N)$$

In this fuzzy logic system, all membership functions are triangular in shape, illustrated in Figure 4. The input and output variables are defined using five FLC sets: NB, NS, ZE, PS, and PB.

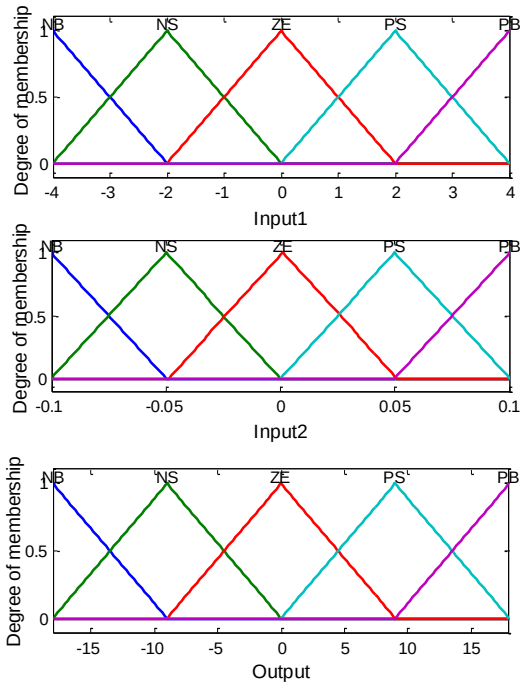

Figure 4. Membership functions corresponding to the input and output variables of the FLC.

Based on the input and output linguistic variables described above, along with their corresponding membership functions, a total of $5 \times 5 = 25$ fuzzy rules are employed to control the D-P OC system. The initial ten fuzzy rules are depicted in Figure 5, while the corresponding input–output mapping of the FLC in three-dimensional space is presented in Figure 6.

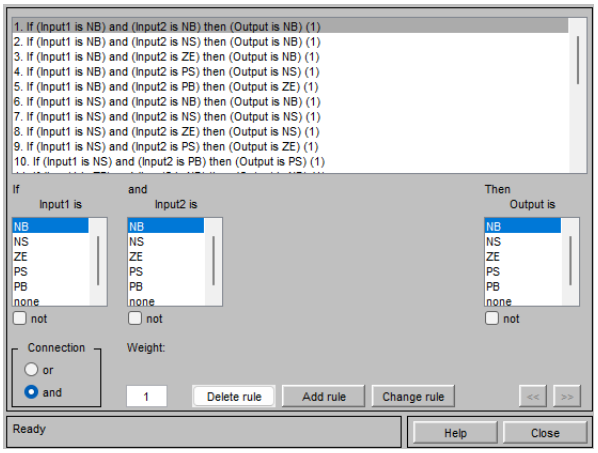

Figure 5. Fuzzy I-T rule base for the FLC.

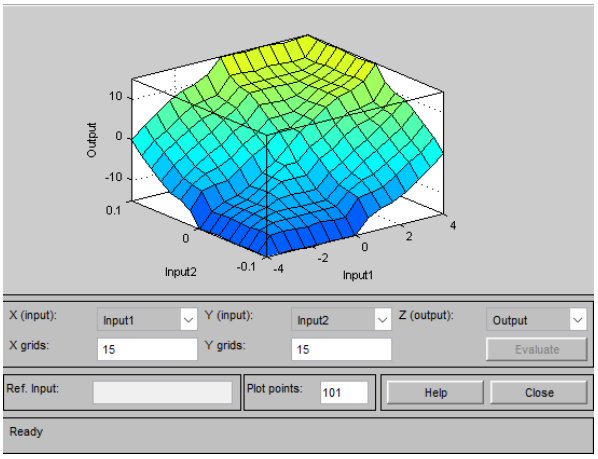

Figure 6. Graphical representation of the input–output relationship of the FLC.

3.2. Design of the PID Controllers

For the OC system model, the second Ziegler–Nichols method combined with a GA is employed to determine the optimal parameters of the PID controllers.

Step 1. Define the structure and parameters to be optimized:

The PID controller is designed to ensure high precision as the system approaches the desired setpoint. The time-domain expression of the PID control law is given as follows:

$$u_{PID}(t) = \sum_{i=1}^{2} u_{PIDi}(t)$$

$$= \sum_{i=1}^{2} k_{PGi}\left(\varepsilon_i(t) + \frac{1}{Z_{IGi}}\int_0^t \varepsilon_i(t)dt + Z_{DGi}\frac{d\varepsilon_i(t)}{dt}\right) \quad (33)$$

Here, $\varepsilon_i(t)$ refers to the input signal, u_{PIDi} is the corresponding output signal, k_{PGi} stands for the proportional gain, Z_{IGi} for the integral time constant, and Z_{DGi} for the derivative time constant.

The transfer functions of the two PID controllers are expressed as follows:

$$G_{ci}(s) = k_{PGi} + \frac{k_{IGi}}{s} + k_{DGi}s \quad (34)$$

The PID parameters to be determined through optimization are:

$$\Delta_i = [k_{PGi}, k_{DGi}, k_{IGi}]$$

Step 2. Formulation of the objective function:

The objective function employed for tuning both PID controllers is given by:

$$J = \varepsilon_1^2(t) + \varepsilon_2^2(t) \rightarrow min \quad (35)$$

The role of the GA is to determine the optimal parameters $(k_{PGi}, k_{DGi}, k_{IGi})$ for both PID controllers, such that the objective function $J$is minimized.

Step 3. Define the search space for the PID parameters:

To constrain the GA search space and reduce computation time for tuning the PID controllers, it is assumed that the optimal values $(k_{PGi}, k_{DGi}, k_{IGi})$ lie approximately around the values $(k_{PZi}, k_{IZi}, k_{DZi})$ obtained from the second Ziegler–Nichols method. The initial random populations are therefore limited as follows:

$$k_{PGi} \in [k_{DZi} - k_{PZi}, k_{DZi}],$$
$$k_{DGi} \in [k_{DZi}, k_{DZi} + k_{PZi}],$$
$$k_{IGi} \in \left[0, \frac{k_{PGi}}{k_{DZi}}\right],$$

In the case where $x\_ri = 1$ and $x\_r(j+1) = 0$, the initial gains k_{IZ1}, k_{IZ2}, k_{DZ1}, k_{DZ2}, and k_{PZ2} are set to zero. The value of k_{PZ1} is increased progressively until it reaches its critical point k_{u1}, at which point the open-loop response begins to oscillate. Using the critical gain k_{u1} together with the corresponding oscillation period Z_{u1}, the PID parameters are calculated according to the relationships proposed by Ziegler–Nichols:

$$k_{PZi} = 0.6k_{ui} \quad (36)$$

$$Z_{IZi} = \frac{1}{2}T_{ui} \quad (37)$$

$$Z_{DZi} = \frac{1}{8}T_{ui} \quad (38)$$

Step 4. GA chromosome representation:

Each member of the genetic algorithm population is encoded as a chromosome:

$$X_i = [k_{PGi}, k_{DGi}, k_{IGi}]$$

The GA parameters are represented as real numbers to improve precision and accelerate convergence.

Step 5. Initial population generation:

The initial population, consisting of N individuals, is randomly generated within the defined search space:

$$X_i^{(0)} = \left\{X_{1i}^{(0)}, X_{2i}^{(0)}, \ldots X_{Ni}^{(0)}\right\}$$

The initial population must exhibit sufficient diversity to avoid convergence to local optima.

Step 6. Fitness evaluation:

The PID parameters corresponding to each individual are assigned to the two controllers, the system is simulated in the time domain, and the objective function $J$is computed.

The fitness value is then determined as follows:

$$F = \frac{1}{1+J} \quad (39)$$

Step 7. Selection and Crossover:

High-fitness individuals are preferentially selected for the next generation. Selection strategies such as Roulette Wheel, Tournament, and Rank Selection help retain the most promising individuals while promoting genetic variation.

Crossover is performed between selected pairs of individuals with a probability P_c to exchange genetic information:

$$X_{offspring} = \alpha X_{parent1} + (1-\alpha) X_{parent2} \quad (40)$$

Where: $\alpha \in [0,1]$ denotes the crossover factor.

Step 8. Mutation Operation:

A mutation is performed with probability $P_m$to randomly modify one or several genes:

$$k_{PGi} = k_{PGi} + \Delta k_i \quad (41)$$

Mutation serves to prevent premature convergence and expand the search within the solution space.

Step 9. Formation of the New Generation and Stopping Criteria:

A new population is generated from the offspring and a portion of the best individuals from the previous generation (elitism). Termination occurs when the maximum generation limit is met or the objective function no longer improves significantly.

Step 10. Selection of Optimal PID Parameters:

The best-performing individual, based on the lowest objective function or highest fitness, defines the optimal PID parameters:

$$(k_{PGi}^*, k_{DGi}^*, k_{IGi}^*)$$

The genetic algorithm (GA) was implemented in M/S to serve as an optimization tool, aiming to determine the optimal parameters for the two PID controllers that satisfy the objective function defined in (35). GA settings for this study: 1500 generations, population size 5000, crossover rate 0.6, mutation rate 0.4.

The optimization yielded the following PID parameters: k_{PG1} = 50.2; k_{IG1} = 0.02; k_{DG1} = 96.1; k_{PG2} = 38.2; $k_{I\text{-}GA2}$ = 0.02; $k_{D\text{-}GA2}$ = 68.9.

4. SIMULATION RESULTS AND ANALYSIS

The FLC-PID controller was implemented and simulated in M/S, employing the system parameters from Table 1. The simulations used reference inputs of $x\_ri = 1$ and $x\_r(j+1) = 0$, with no external disturbance $d(t) = 0$ N.

Simulation outcomes are shown in Figures 7 and 8. Here, x_{1-PID}, y_{1-PID},y_{2-PID}, u_{PID} , $x_{1-FLC-PID}$, $y_{1-FLC-PID}$,$y_{2-FLC-PID}$, $u_{FLC-PID}$ correspond to the response trajectories of the T P, HSA, PSA, and the control input for the OC system under PID and FLC-PID control, respectively. The simulation outcomes are quantitatively compared in Table 2.

The combined swing indices $J_{y\text{-PID}}$ and $J_{y\text{-FLC-PID}}$quantify the cumulative oscillation over time of the entire D-P system (H&P) and are given by the following expressions:

$$J_{y-PID} = \int_0^T \begin{pmatrix} y_{1-PID}^2(t) \\ +y_{2-PID}^2(t) \end{pmatrix} dt = 0.0131 \quad (42)$$

$$J_{y-FLC-PID} = \int_0^T \begin{pmatrix} y_{1-FLC-PID}^2(t) \\ +y_{2-FLC-PID}^2(t) \end{pmatrix} dt = 0.0109 \quad (43)$$

The results show that the proposed FLC–PID controller attains the minimum value of J_y ("FLC-PID"), indicating better vibration suppression performance than conventional PID.

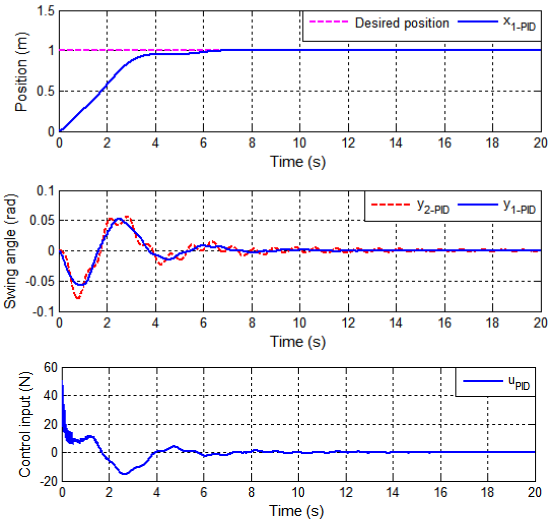

Figure 7. OC System Simulation Using a Standard PID Controller

Equations (42) and (43) along with Table 2 indicate that the FLC–PID control structure significantly enhances control performance compared to the conventional PID controller. Specifically, the trolley settling time is reduced by approximately 32.4%, while both the amplitude and duration of hook and payload oscillations are substantially decreased. Moreover, the peak control force in the FLC–PID case is lower, demonstrating higher control efficiency and better suitability for practical overhead crane applications.

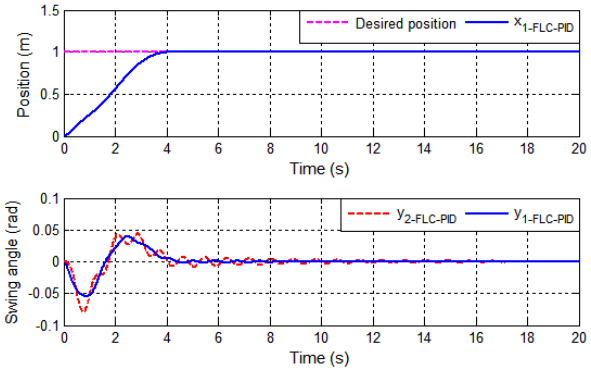

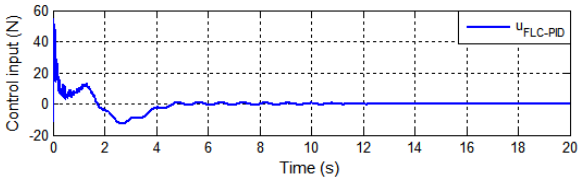

Figure 8. OC system simulation using an FLC

Table 2. Comparison of control performance between PID and FLC–PID controllers

Symbol	PID	FLC-PID
Desired position, x_r1(m)	1	1
Overshoot, POT(%)	0	0
Steady-state error, e_{xl}(%)	0	0
Position settling time, t_{x1}(s)	6.8	4.1
Hook swing settling time, t_{y1}(s)	12	6.5
Maximum hook swing angle, y_{1max}(rad)	0.055	0.05
Maximum payload swing angle, y_{2max}(rad)	0.075	0.068

Moreover, the OC system experiences external disturbances while operating. Notably, at startup, the crane experiences significant friction forces and payload impacts, resulting in strong P O. To assess the performance reliability of the FLC-PID controller, the authors assume step-type disturbance signals [15] as follows: In Case 1, a friction-induced disturbance with an amplitude of $d_1 = -10$ N acts for 2 s immediately at system startup; in Case 2, a payload collision disturbance with an amplitude of $d_2 = 20$ N is applied for 2 s at $t = 10$ s.

Simulation outcomes are shown in Figures 9 and 10. Here, the variables $x_{1d1}, y_{1d1}, y_{2d1}, u_{d1}$, $x_{1d2}, y_{1d2}, y_{2d2}, u_{d2}$represent the system responses under the respective disturbance conditions. These response curves closely follow the corresponding responses x_1, y_1, y_2, u obtained under disturbance-free conditions. The system demonstrates robustness, as its behavior is hardly altered by disturbances, demonstrating that the FLC-PID

controller reliably maintains the desired control performance.

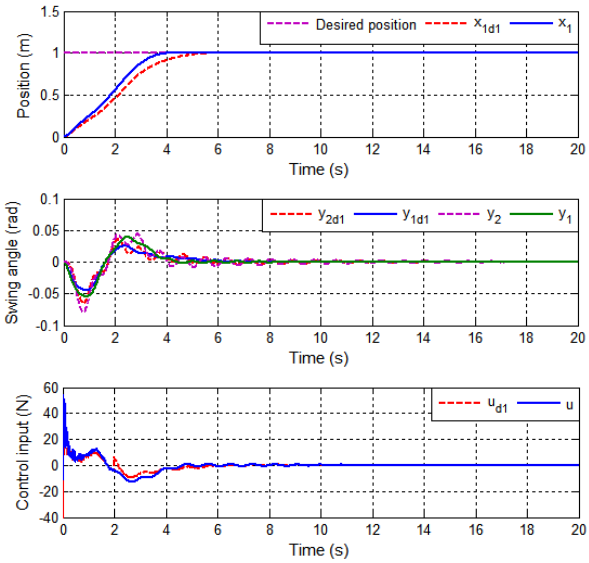

Figure 9. Simulated response of the OC system under disturbance in Case 1.

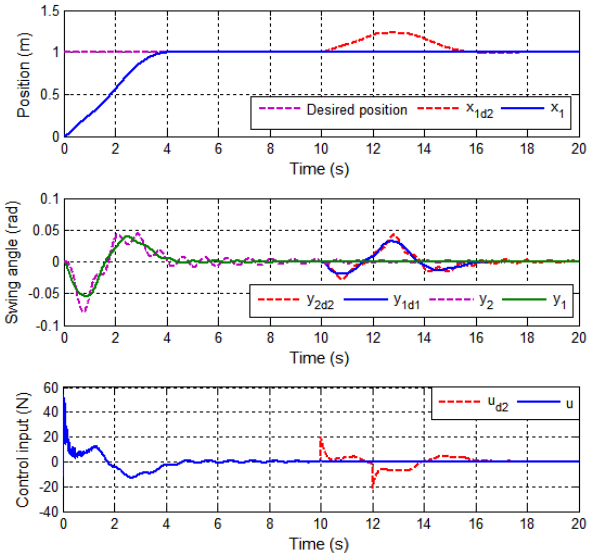

Figure 10. Simulation of the OC system's response under disturbance in Case 2.

In practical operations, the overhead crane system often experiences variations in parameters such as payload mass and hoist cable length depending on working conditions. To more accurately reflect real-world scenarios and assess the impact of parameter changes on the performance of the FLC-PID controller, the authors modified the payload mass to $m_2 = 0.8$ kgand the hoist cable length to $l_2 = 0.4$ m, while keeping all other parameters in Table 1 unchanged. The simulation results are shown in Figure 11. The results indicate that the system responses under the modified m_2 and l_2 conditions closely track those obtained with the nominal parameters. This demonstrates that the system maintains high control quality and that the FLC-PID controller exhibits robustness and adaptability to variations in system parameters.

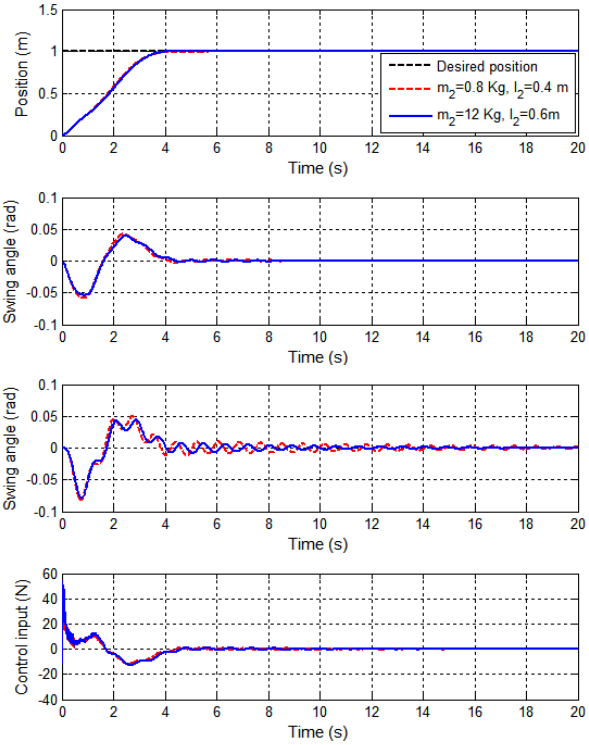

Figure 11. Simulated response of the OC system with varying m_2 and l_2.

To highlight the advantages of the proposed approach, the authors conducted a comparative analysis of the FLC-PID controller against other control methods reported in previous studies, as summarized in Table 3.

The data presented in Table 3 indicate that the Adaptive Tracking Control (ATC) approach [7] results in the smallest maximum SA $y_{1\max}$ and $y_{2\max}$; however, the settling time $t_{x1}$is relatively long. The GA-FLC [3] and SMC [10] approaches exhibit higher values for $y_{2\max}$, t_{x1} . In contrast, the proposed FLC-PID controller achieves comparatively low values for all three performance indicators $y_{1\max}$, $y_{2\max}$, and t_{x1}. These results indicate that while all the compared control methods are capable of maintaining acceptable system performance, the FLC-PID controller demonstrates a clear advantage for the D-P OC studied in this paper,

providing superior trolley positioning control while effectively suppressing both H&P oscillations.

Table 3. Comparison of FLC-PID performance with previously published controllers

Symbol	FLC-PID	GA-FLC [3]	ATC [7]	SMC [10]
x_r1	1 m	1m	1 m	10 m
POT	0 %	0 %	0 %	0 %
e_{xl}	0 %	0 %	0 %	0 %
t_{x1}	4.1 s	7.1 s	7 s	5.2 s
t_{y1}	6.5 s	6.8 s	6.5 s	6.5 s
y_{1max}	0.05 rad	0.06 rad	0.022 rad	0.48 rad
y_{2max}	0.068 rad	0.07 rad	0.024 rad	0.69 rad

5. CONCLUSION

In this paper, an FLC-PID control structure, consisting of a FLC combined with two PID controllers whose parameters are optimized using a GA, has been proposed for positioning control of the T while simultaneously suppressing the angular O of the H&P in an OC system. The performance of the proposed controller was assessed through simulations carried out in the M/S environment. The results indicate that the system attains the desired control objectives with zero overshoot (POT = 0%), a T P settling time of $t_{x1} = 4.1$ s, a maximum HSA of $y_{1\max} = 0.05$ rad, a maximum PSA of $y_{2\max} = 0.068$ rad, and a maximum control force of $u_{\max} = 45$ N applied within $t_u = 10$ s. These findings confirm that the proposed controller ensures stable system responses and superior control performance. Furthermore, to assess the reliability and robustness of the proposed approach, simulations were carried out under external disturbances and parameter variations. The results indicate that the FLC-PID controller maintains high positioning accuracy while effectively limiting the SA of both the H&P. In future work, the proposed FLC-PID controller will be experimentally validated on a real OC system to evaluate its effectiveness under practical operating conditions and system uncertainties. In addition, adaptive and self-tuning control mechanisms, as well as alternative optimization algorithms such as PSO, DE, or hybrid metaheuristic approaches, will be investigated to further enhance the controller's performance and scalability for more complex OC systems.

REFERENCES

1. Van Trung Nguyen; Chunhua Yang, Ph.D; Chenglong Du; Liqing Liao, Ph.D (2019). *Design and Implement of Finite-Time Sliding Mode Controller for Fuzzy Overhead Crane System*. ISATRANS-D-19-00899.
2. Ernesto Molina-Santana, Michel Roberto Ferrer-Cepero, Felipe Gonzalez-Montañez, Jesús Ulises Liceaga-Castro, Victor M. Jimenez-Mondragon, Juan Carlos Olivares-Galvan (2025). *Generalized framework for designing a linear control scheme for regulating a sub-actuated overhead crane*. International Journal of Dynamics and Control 13:168.
3. Dianwei Qian, Shiwen Tong, SukGyu Lee (2016), *Fuzzy-Logic-based control of payloads subjected to double-pendulummotion in overhead cranes*, Automation in Construction 65, 133–143.
4. S. Zhang, X. He, H. Zhu, Q. Chen, and Y. Feng, (2020), *Partially saturated coupled-dissipation control for underactuated overhead cranes,* Mechanical Systems and Signal Processing 136: 106449. DOI 10.1016/j.ymssp.2019.106449.
5. M. R. Mojallizadeh, B. Brogliato, and C. Prieur, (2023), *Modeling and control of overhead cranes: A tutorial overview and perspectives,* Annual Reviews in Control 56: 100877. DOI 10.1016/j.arcontrol.2023.03.002.
6. G. Rigatos, (2023), *Nonlinear optimal control for the underactuated double-pendulum overhead crane*, Journal of Vibration Engineering & Technologies: 1–21. DOI 10.1007/s42417-023-00902-y.

7. Menghua Zhang, Xin Ma, Xuewen Rong, Xincheng Tian, Yibin Li (2016), *Adaptive tracking control for double-pendulum overheadcranes subject to tracking error limitation, parametricuncertainties and external disturbances*, Mechanical Systems and Signal Processing 76-77, 15–32.
8. Y.C. Fang, B.J. Ma, P.C. Wang, and X.B. Zhang (2012), *A motion planning-based adaptive control method for an underactuatedcrane system*, IEEE Transactions on Control Systems Technology 20 (1), 241–248.
9. Khalid L. Sorensen, William Singhose, Stephen Dickerson (2007). *A controller enabling precise positioning and sway reduction in bridge and gantry cranes.* Control Engineering Practice 15, 825–837.
10. Nguyễn Văn Trung, Bùi Thị Thêm, Phí Thị Thanh Huyền (2025). *Design of sliding controller using lyapunov stability theory for control of double pendulum gantry crane*. Tạp chí Khoa học và Công nghệ QUI, số 2. ISSN 2815-6145
11. Diantong Liu, Jianqiang Yi, Dongbin Zhao, Wei Wang (2005). *Adaptive sliding mode fuzzy control for atwo-dimensional overhead crane.* Mechatronics 15, 505–522.
12. Manh-Linh Nguyen, Hoang-Phat Nguyen, and Thi-Van-Anh Nguyen∗ (2024). *H-Infinity Approach Control On Takagi-Sugeno Fuzzy Model For 2-D Overhead Crane System*. Journal of Applied Science and Engineering, Vol. 28, No 5, Page 995-1003.
13. D. Qian, S. Tong, B. Yang, and S. Lee (2015). *Design of simultaneous input-shaping-based SIRMs fuzzy controlfor double-pendulum-type overhead cranes.* BULLETIN OF THE POLISH ACADEMY OF SCIENCESTECHNICAL SCIENCES, Vol. 63, No. 4. *DOI: 10.1515/bpasts,887-896*.
14. Naif B. Almutairi and Mohamed Zribi (2016). *Fuzzy Controllers for a Gantry Crane System with Experimental Verifications.* Article in Mathematical Problems in Engineering. DOI: 10.1155/1965923.
15. Mahmud Iwan Solihin, Wahyudi, Ari Legowo and Rini Akmeliawati (2009), *Robust PID Anti-swing Control of Automatic GantryCrane based on Kharitonov's Stability*, P.O. Box 10, 50728. Kuala Lumpur, Malaysia, 978-1-4244-2800-7/09/$25.00, IEEE.
16. Mohammad Javad Maghsoudi, Z. Mohamed, A.R. Husain, M.O. Tokhi (2016), *An optimal performance control scheme for a 3D crane,* Mechanical Systems and Signal Processing 66-67, 756–768.
17. Zhe Sun, Ning Wang, Yunrui Bi, Jinhui Zhao (2015), *A DE based PID controller for two dimensional overhead crane,* Proceedings of the 34th Chinese Control ConferenceJuly 28-30, Hangzhou, China, 2546-2550.
18. Nguyễn Văn Trung, Phạm Đức Khẩn, Phạm Thị Thảo, Lương Thị Thanh Xuân (2017), *Ứng dụng giải thuật di truyền thiết kế hai bộ điều khiển PID để điều khiển giàn cần trục cho điện phân đồng.* Tạp chí Nghiên cứu khoa học - Đại học Sao Đỏ, ISSN 1859-4190. Số 3(58).
19. Mahmud Iwan Solihin and Wahyudi (2007), *Fuzzy-tuned PID Control Design forAutomatic Gantry Crane,* P.O. Box 10. 50728.Kuala Lumpur, Malaysia, 1-4244-1355-9/07/$25.00, IEEE.
20. E. A. Esleman, G. Önal, and M. Kalyoncu (2021). *Optimal PID and fuzzy logic based position controller design of an overhead crane using the Bees Algorithm*. SN Applied Sciences 3(10): 811. DOI: https://doi.org/10.1007/s42452-021-04793-0.

Thông tin của tác giả:
TS. Nguyễn Văn Trung
Trường Đại học Công nghiệp Quảng Ninh
Điện thoại: +(84).988.941.166 - Email: ngvtrung1982@gmail.com
ThS. Nguyễn Thị Phúc
Trường Đại học Công nghiệp Quảng Ninh
Điện thoại: +(84). 977 512 911 - Email: phucqui.edu.vn@gmail.com
ThS. Phí Thị Thanh Huyền
Trường Đại học Công nghiệp Quảng Ninh

Điện thoại: +(84).982.932.468 - Email: phihuyen.83@gmail.com
KS. Trần Thị Duyên
Trường Đại học Công nghiệp Quảng Ninh
Điện thoại: +(84).977203343- Email: duyentk50@gmail.com
KS. Đỗ Minh Hiếu
Công Ty TNHH điện lực AES Mông Dương
Điện thoại: 0366131953 - Email: hieu.do@aes.com

THIẾT KẾ VÀ TỐI ƯU HÓA BỘ ĐIỀU KHIỂN FUZZY-PID SỬ DỤNG THUẬT TOÁN DI TRUYỀN ĐỂ ĐIỀU KHIỂN CẦN CẨU TRÊN CAO

Information about authors:
Nguyen Van Trung, Ph.D., Quang Ninh University of Industry, email: ngvtrung1982@gmail.com
Nguyen Thi Phuc, M.Sc., Quang Ninh University of Industry, email: phucqui.edu.vn@gmail.com
Phi Thi Thanh Huyen, M.Sc., Quang Ninh University of Industry, email: phihuyen.83@gmail.com
Tran Thi Duyen, B.Eng., Quang Ninh University of Industry, email: duyentk50@gmail.com
Do Minh Hieu, B.Eng., AES Mong Duong Power Company Limited, email: hieu.do@aes.com

TÓM TẮT

Cần cẩu trên cao (OC) là một hệ thống cơ điện có động lực học phi tuyến và bị ảnh hưởng đáng kể bởi dao động tải (LO), thường được mô hình hóa như một hệ thống con lắc kép (D-P). Dao động (O) của móc và tải trọng (H&P) làm giảm độ chính xác định vị (P) của xe đẩy (T) và có thể dẫn đến hư hỏng cơ khí và nguy hiểm về an toàn. Để giảm thiểu những hạn chế này, một sơ đồ điều khiển kết hợp FLC–PID được giới thiệu nhằm mục đích cải thiện hiệu suất hoạt động của OC. Trong sơ đồ đề xuất, bộ điều khiển mờ tăng cường phản ứng động của hệ thống dưới các sai số theo dõi lớn, do đó đảm bảo định vị nhanh chóng T tại vị trí mong muốn. Bộ điều khiển PID đảm bảo tính ổn định của hệ thống khi T tiến gần đến điểm đặt, sử dụng thuật toán di truyền (GA) để tối ưu hóa các tham số nhằm triệt tiêu dao động và tăng cường độ chính xác P. Hiệu quả của phương pháp đề xuất được xác thực thông qua mô phỏng MATLAB/Simulink. Kết quả mô phỏng cho thấy độ chính xác P được cải thiện, giảm đáng kể dao động H&P O, và phản hồi hệ thống nhanh chóng, ổn định.

Từ khóa: *Cần cẩu trên cao; Điều khiển mờ và PID; Thuật toán di truyền; Điều khiển dao động; vị trí.*

Ngày nhận bài: 24/12/2025;
Ngày nhận bài sửa: 26/12 /2025;
Ngày chấp nhận đăng: 28/12/2025.